

Draft November 8, 2018

# OBSERVATIONS OF MASS LOSS FROM THE TRANSITING EXOPLANET HD 209458b <sup>1</sup>

Jeffrey L. Linsky

*JILA, University of Colorado and NIST, 440 UCB Boulder, CO 80309-0440*

`jlinsky@jilau1.colorado.edu`

Hao Yang

*JILA, University of Colorado and NIST, 440 UCB Boulder, CO 80309-0440*

`haoyang@jilau1.colorado.edu`

Kevin France

*CASA, University of Colorado, 593 UCB Boulder, CO 80309-0593*

`Kevin.France@colorado.edu`

Cynthia S. Froning

*CASA, University of Colorado, 593 UCB Boulder, CO 80309-0593*

`cfroning@casa.colorado.edu`

James C. Green

*CASA, University of Colorado, 593 UCB Boulder, CO 80309-0593*

`James.Green@colorado.edu`

John T. Stocke

*CASA, University of Colorado, 593 UCB Boulder, CO 80309-0593*

`stocke@casa.colorado.edu`

Steven N. Osterman

*CASA, University of Colorado, 593 UCB Boulder, CO 80309-0593*

steven.osterman@colorado.edu

## ABSTRACT

Using the new Cosmic Origins Spectrograph (COS) on the *Hubble Space Telescope* (*HST*), we obtained moderate-resolution, high signal/noise ultraviolet spectra of HD 209458 and its exoplanet HD 209458b during transit, both orbital quadratures, and secondary eclipse. We compare transit spectra with spectra obtained at non-transit phases to identify spectral features due to the exoplanet’s expanding atmosphere. We find that the mean flux decreased by  $7.8 \pm 1.3\%$  for the C II 1334.5323 Å and 1335.6854 Å lines and by  $8.2 \pm 1.4\%$  for the Si III 1206.500 Å line during transit compared to non-transit times in the velocity interval  $-50$  to  $+50$  km s<sup>-1</sup>. Comparison of the C II and Si III line depths and transit/non-transit line ratios shows deeper absorption features near  $-10$  and  $+15$  km s<sup>-1</sup> and less certain features near  $-40$  and  $+30$ – $70$  km s<sup>-1</sup>, but future observations are needed to verify this first detection of velocity structure in the expanding atmosphere of an exoplanet. Our results for the C II lines and the non-detection of Si IV 1394.76 Å absorption are in agreement with Vidal-Madjar et al. (2004), but we find absorption during transit in the Si III line contrary to the earlier result. The  $8 \pm 1\%$  obscuration of the star during transit is far larger than the 1.5% obscuration by the exoplanet’s disk. Absorption during transit at velocities between  $-50$  and  $+50$  km s<sup>-1</sup> in the C II and Si III lines requires high-velocity ion absorbers. Assuming hydrodynamic model values for the gas temperature and outflow velocity at the limb of the outflow as seen in the C II lines, we find mass-loss rates in the range  $(8\text{--}40) \times 10^{10}$  g s<sup>-1</sup>. These rates assume that the carbon abundance is solar, which is not the case for the giant planets in the solar system. Our mass-loss rate estimate is consistent with theoretical hydrodynamic models that include metals in the outflowing gas.

*Subject headings:* planets and satellites: atmospheres — planets and satellites: individual (HD 209458b) — planets and satellites: physical evolution — stars: individual (HD 209458) — ultraviolet: stars

---

<sup>1</sup>Based on observations made with the NASA/ESA *Hubble Space Telescope*, obtained from the Data Archive at the Space Telescope Science Institute. STScI is operated by the Association of Universities for Research in Astronomy, Inc., under NASA contract NAS 5-26555. These observations are associated with the *HST* GTO program #11534.

## 1. INTRODUCTION

Mazeh et al. (2000) monitored the radial velocities of the G0 V star HD 209458 to derive the orbital parameters and minimum mass of its transiting planet HD 209458b. Very shortly thereafter, accurate measurements of the mass and radius of HD 209458b were extracted from radial velocity and photometric transit observations by Henry et al. (2000) and Charbonneau et al. (2000). Table 1 lists the presently accepted properties of HD 209458 and HD 209458b cited by Knutson et al. (2007). HD 209458b is likely the best-studied Jupiter-like exoplanet located very close to its host star. As a result of its proximity, HD 209458b receives very strong incident radiation (see estimate in Table 1) and stellar wind flux from its host star.

HD 209458b is the first transiting planet for which atmospheric absorption was observed in the resonance lines of Na I (Charbonneau et al. 2002) and subsequently in lines of H I, C II, O I, and others. Using the G140M grating of Space Telescope Imaging Spectrograph (STIS) on the Hubble Space Telescope *HST* with its resolution of  $\sim 30 \text{ km s}^{-1}$ , Vidal-Madjar et al. (2003) found that the Lyman- $\alpha$  line flux was reduced by  $15 \pm 4\%$  during transit at velocities between  $-130$  and  $+100 \text{ km s}^{-1}$ . Based on this first detection of H I absorption at or above the planet’s Roche lobe, they concluded that hydrogen is escaping from the planet. Vidal-Madjar et al. (2004) then used the low-resolution G140L grating of STIS to detect an absorption depth at midtransit of  $5 \pm 2\%$  for the unresolved Lyman- $\alpha$  line,  $13 \pm 4.5\%$  for the O I 1304 Å multiplet, and  $7.5 \pm 3.5\%$  for the C II 1335 Å doublet. Their detection of absorption in the O I and C II lines at or above the Roche lobe confirmed significant mass loss from the planet by hydrodynamic outflow. They argued that reduction in the Lyman- $\alpha$  line flux at  $\approx 100 \text{ km s}^{-1}$  from line center indicates high velocities of neutral hydrogen atoms. Additionally, more absorption on the blue side of the Lyman- $\alpha$  emission line than the red side indicates outflow towards the observer and away from the planet. A subsequent observation of HD 209458 using the *HST* Advanced Camera for Surveys (ACS) showed a reduction in the unresolved Lyman- $\alpha$  line flux of  $(8.0 \pm 5.7)\%$  during transits, consistent with the STIS G140L and G140M results, thereby confirming mass loss from the planet’s large exosphere (Ehrenreich et al. 2008).

There have been a number of reanalyses of the data and further discussions of the STIS transit G140M observations by Ben-Jaffel (2007), Ben-Jaffel (2008), Vidal-Madjar et al. (2008) and others. There is a consensus that HD 209458b has an extended exosphere and is losing mass, but important details are not yet understood. Such questions as: whether the exosphere size is larger or smaller than the projected Roche lobe, what are the outflow speed and mass-loss rate, and whether or not the mass loss from the planet produces a cometlike tail are not yet answered with the existing STIS and ACS observations. While

the STIS G140M Lyman- $\alpha$  spectrum obtained by Vidal-Madjar et al. (2003) provides some velocity information, higher spectral resolution and signal/noise (S/N) are needed to obtain the velocity structure and optical depth of the outflowing gas in Lyman- $\alpha$  and other spectral lines.

The large abundance of hydrogen and large flux in the Lyman- $\alpha$  line make this line a prime candidate for studying exoplanet outflows, but there are uncertainties (many of them unique) in measuring the exoplanet’s mass-loss rate only from this line. These include the modest S/N of the existing STIS G140M grating data, possible variability of the stellar Lyman- $\alpha$  profile at the time of transit that cannot be directly measured, broad interstellar absorption in the core of the line that prevents measurements of low velocity absorption during transit, and the time-varying geocoronal and interplanetary emission in the line core that cannot be completely corrected for.

Absorption of Lyman- $\alpha$  photons during transit over the velocity range  $-130$  to  $+100$   $\text{km s}^{-1}$  raises the question of the origin of the high-velocity hydrogen that is difficult to explain by a thermal plasma at moderate temperature. Holmström et al. (2008) proposed that the high-velocity neutral hydrogen can be produced by charge exchange between stellar wind protons and neutral hydrogen in the planet’s outflow. Such energetic neutral atoms (ENAs) are seen in the solar system and likely occur where the stellar and planetary winds interact between HD 209458b and its host star. If this were the only possible explanation, then the Lyman- $\alpha$  profile during transit provides useful information on the stellar wind but ambiguous information on mass loss from the planet (Holmström et al. 2008; Murray-Clay et al. 2009). However, Lecavelier des Etangs et al. (2008b) argued that the observed Lyman- $\alpha$  profile and the high-velocity hydrogen atoms can be simply explained by stellar radiation pressure and the ENA explanation required a peculiar stellar wind model.

The Lyman- $\alpha$  transit observations by Vidal-Madjar et al. (2003, 2004) stimulated a number of interpretive papers concerning the mechanisms for mass loss and lifetime of a Jupiter-like planet close to its host star [e.g., Vidal-Madjar et al. (2003); Baraffe et al. (2004); Koskinen et al. (2007); Holmström et al. (2008); Koskinen et al. (2010)] and hydrodynamic models [e.g., Lammer et al. (2003); Lecavelier des Etangs et al. (2004); Yelle (2004); Jaritz et al. (2005); Tian et al. (2005); Garcia Muñoz (2007); Schneider et al. (2007); Murray-Clay et al. (2009)]. As discussed below, the theoretical models differ in their treatment of the amount of available radiative energy input (photoionization and otherwise) to drive the hydrodynamic blow-off, the location of the heating, the presence of metals in the outflow, and the relative amount of cooling by expansion, thermal conduction, and radiation. These models predict very different mass-loss rates. Which of these models are consistent with the spectrally resolved metal lines observed during transit?

With the objectives of measuring an accurate mass-loss rate from the planet and testing different physical models for the mass loss, one needs far better data, which requires a new scientific instrument. One needs higher S/N spectra with higher spectral resolution and sufficient sensitivity to study many spectral lines formed in the extended atmosphere and wind of the exoplanet. In particular, it is important to use spectral lines other than Lyman- $\alpha$  to avoid unique difficulties in the analysis of this line. As we describe below, the new Cosmic Origins Spectrograph (COS) on *HST* is well designed for this task.

## 2. OBSERVATIONS AND DATA REDUCTION

Installed on the *HST* during Servicing Mission 4 in 2009 May, COS is a high-throughput ultraviolet (UV) spectrograph optimized for point sources. Descriptions of the on-orbit performance characteristics of COS will be presented by Green et al. (2010, in preparation) and Osterman et al. (2010, in preparation). During GTO Program 11534, we observed HD 209458 with both the G130M and G160M gratings of the COS far-UV channel to obtain moderate-resolution spectra covering the 1140–1790 Å spectral region. In this paper, we analyze the spectra obtained with the G130M grating, which includes the spectral range 1140–1450 Å. The G160M observations are presented by France et al. (2010). The COS line-spread function (LSF) in the far-UV is not a simple Gaussian, but it can be approximated by a Gaussian with a resolution of 17,000–18,000 (16.7–17.6 km s<sup>-1</sup>) with extended wings (Ghavamian et al. 2010).

We have tested for the effects of the extended wings by comparing the C II 1335.6854 Å emission line of  $\alpha$  Cen A (G2 V) observed with the STIS E140H grating (3 km s<sup>-1</sup> resolution) convolved with a Gaussian (17 km s<sup>-1</sup> resolution) and with the COS LSF. In the line wings at 50–70 km s<sup>-1</sup>, the Gaussian broadens the profile by less than 1 km s<sup>-1</sup>, but the COS LSF broadens the profile by 2–6 km s<sup>-1</sup>. Since both the transit and non-transit line profiles are broadened in the same way, their ratio is not changed by the broad wings of the COS LSF. The broadening of the intrinsic spectral lines by the COS LSF (compared to the Gaussian profile) is less than 1/3 of the spectral resolution element and thus not significant.

Table 2 summarizes the individual G130M exposures obtained at transit (near orbital phase 0.00), first quadrature (phase 0.25), secondary eclipse (phase 0.50), and second quadrature (phase 0.75). The total exposure times for these phases are 4946.8 s, 7941.7 s, 4956.7 s, and 7796.0 s, respectively. The orbital phases listed in Table 2 are computed using the ephemeris of Knutson et al. (2007). Transit occurs between orbital phases 0.982 and 0.018 (Wittenmyer et al. 2005) as indicated by the optical light curve. Since the duration of transit is about 3.22 hours, *HST* could observe HD 209458 during the same transit on two sequential

spacecraft orbits.

The S/N in the COS spectra can be lower than predicted by photon statistics as a result of two instrumental effects. The hex pattern formed at the intersection of the microchannel plate pores imposes a  $\pm 4\%$  pattern on the spectral signal, and shadows of the wire grid on the detector decrease the signal as much as 20% at certain locations on the detector faceplate. We checked the locations of the known wire grid shadows and found that the spectra of the C II, Si III, and Si IV lines studied in this paper are not affected by the wire grids. Both effects, which are fixed at the detector, were mitigated by moving the grating and the resultant spectrum to different positions on the detector. In this program, we observed at four different grating offset positions identified by the beginning and ending wavelengths of the gap between the two detector faceplate elements listed in the last column of Table 2. In principle, division of a transit spectrum by a non-transit spectrum at the same grating position should cancel the signal errors introduced by both instrumental effects to show the true spectral difference produced by the planet in front of the star. In practice, the cancellation will not be perfect because of possible time variations in the stellar spectrum and grating mechanisms that do not return to the same position every time. The grating mechanism positioning errors are not fully understood at this time. We found that the wavelength solutions for spectra observed at different grating offset positions are not identical and could be off by 1–2 pixels. We registered each observed spectrum with others at the same grating setting by cross-correlating the interstellar feature in the C II 1334.5323 Å line. These registrations typically involved displacements by only 1–2 pixels, far less than a resolution element with no significant degradation in the spectral resolution. We then co-added the summed spectra for the four grating offset positions using the same cross-correlation technique. Also, within 500 pixels of the end of each detector segment (about 5 Å for G130M), there are additional instrumental artifacts in the spectrum. For this reason, we did not analyze portions of the spectrum near the ends of a detector faceplate. The data were processed with the COS calibration pipeline, CALCOS<sup>2</sup> v2.11b (2009-09-08) and combined with a custom IDL coaddition procedure.

Figure 1 shows a portion of the G130M spectra obtained during transit and all non-transit phases (secondary eclipse and both quadratures). The spectra are very similar, but there are subtle differences that provide information on the exoplanet’s atmosphere and mass-loss rate. In this paper, we compare transit and non-transit spectra of lines of C II, Si III, and Si IV. The H I Lyman- $\alpha$  line cannot be analyzed because geocoronal emission through the large aperture of COS completely dominates any stellar component. The O I

---

<sup>2</sup>We refer the reader to the cycle 18 COS Instrument Handbook for more details: [http://www.stsci.edu/hst/cos/documents/handbooks/current/cos\\_cover.html](http://www.stsci.edu/hst/cos/documents/handbooks/current/cos_cover.html).

lines at 1302, 1304, and 1306 Å were also not analyzed because time-varying geocoronal emission in these lines renders comparison of transit and non-transit spectra uncertain and because the lines were located close to the end of a detector faceplate.

### 3. RESULTS

#### 3.1. *Si IV Line*

A critical question is whether the emission line fluxes of the host star were significantly different at the times when the transit and non-transit spectra were obtained, since late-type stars like the Sun often show time-variable emission in lines formed in their outer atmospheres (e.g., Rottman 2006). Figure 2 shows the co-added transit and non-transit spectra for the Si IV resonance line (1393.76 Å). Since the Si IV line is formed in highly ionized gas which is not likely to be in the atmosphere or extended wind of the exoplanet, the very similar Si IV fluxes during times of transit and non-transit indicate that the average flux in the stellar emission lines during our observations was nearly constant. The difference spectrum panel in Figure 2 confirms that the transit and non-transit spectra of the Si IV line are identical to within the noise level.

To make the comparison of the transit and non-transit Si IV line profiles more quantitative, we compute the mean transit/non-transit flux ratio over the velocity range  $-50$  to  $+50$  km s $^{-1}$ . Beyond this velocity range, the fluxes are less than 15% of the peak flux, and the S/N in each spectral resolution element is small. For the 100 km s $^{-1}$  wide velocity interval centered on 0 km s $^{-1}$ , the mean flux ratio is 0.998. To estimate the error in the mean flux ratio, we have computed flux ratios for many velocity intervals contained within the  $-50$  to  $+50$  km s $^{-1}$  velocity range that are between 60 and 95 km s $^{-1}$  wide. The dispersion of these flux ratios indicates that the standard deviation in the mean flux ratio for the  $-50$  to  $+50$  km s $^{-1}$  velocity range is  $\pm 0.014$ . We therefore conclude that the mean stellar fluxes in the other emission lines were the same during transit and non-transit times, and do not rescale the transit and non-transit fluxes. At positive velocities, there are regions where the transit/non-transit ratio may differ from unity at or above one standard deviation. We discuss this in Section 3.4.

#### 3.2. *C II Lines*

The C II lines at 1334.5323 Å and 1335.6854 Å are bright emission lines formed in the chromospheres of solar-type stars like HD 209458. On October 2, 2009, we observed the C II

lines during transit with the G130M grating at four grating positions specified by the gap wavelengths listed in Table 2. For each of these grating positions, there are corresponding observations at both quadratures and a secondary eclipse obtained at different times.

Figure 3 shows the co-added spectra of the C II 1334.5323 Å resonance line and the C II 1335.6854 Å line. The spectra were smoothed with a 5-pixel boxcar, which is somewhat smaller than the on-orbit G130M spectral resolution element of 7–8 pixels. The transit and non-transit spectra are plotted separately and ratioed. The deep minimum observed in the C II 1334.5323 Å line at  $-6.60 \text{ km s}^{-1}$  (heliocentric) is interstellar absorption due to the Eri cloud located within 3.5 pc of the Sun (Redfield & Linsky 2008). Since the radial velocity of HD 209458 is  $-14.8 \text{ km s}^{-1}$ , the  $-6.6 \text{ km s}^{-1}$  interstellar absorption is centered to the red of the centroid of the stellar emission line.

Both C II lines show less flux during transit than non-transit times, although there are small velocity intervals where the transit/non-transit ratio exceeds unity. To test whether the ratios in these velocity intervals are real or noise, we have co-added the profiles of the two C II lines (including the portion of the 1334 Å line with interstellar absorption) to get transit and non-transit profiles with twice the signal and higher S/N. The co-added C II profiles are included in Figure 3, together with difference and ratio profiles for each C II line and the co-added line. The co-added C II line shows absorption during transit at all velocities between  $-50$  and  $+50 \text{ km s}^{-1}$ , except at zero velocity. The deep absorption features for the co-added C II line are interesting and will be discussed in Section 3.4.

Using the same method that we used for the Si IV line, we find that the mean flux ratio in the  $-50$  to  $+50 \text{ km s}^{-1}$  velocity interval is  $0.924 \pm 0.022$  for the C II 1334.53 Å line and  $0.921 \pm 0.015$  for the C II 1335.69 Å line. For the co-added C II line, the mean flux ratio is  $0.922 \pm 0.013$ .

### 3.3. *Si III Line*

Figure 2 shows the co-added transit and non-transit spectra for the Si III resonance line at 1206.500 Å. The difference and ratio spectra show absorption at all velocities between  $-60$  and  $+60 \text{ km s}^{-1}$ . There are also deep absorption features which we will discuss in Section 3.4.

Using the same method that we used in analyzing the Si IV and C II lines, we find that the mean flux ratio in the  $-50$  to  $+50 \text{ km s}^{-1}$  band is  $0.918 \pm 0.014$ , the same within errors as previously seen for the C II lines. Our result for the mean absorption depth during transit of  $8.2 \pm 1.4\%$  is very different from the non-detection absorption depth of  $0.0^{+2.2\%}_{-0.0\%}$



obtained by Vidal-Madjar et al. (2004) from the STIS G140L spectrum and confirmed by Ben-Jaffel & Sona Hosseini (2010). We suspect that the difference between our detection of Si III absorption during transit and the previous non-detection is due to time variability. Charge transfer between protons and  $\text{Si}^+$  ions leads to a substantially higher abundance of  $\text{Si}^{++}$  than is the case for collisional ionization equilibrium. Baliunas & Butler (1980) found that  $\text{Si}^{++}$  is the dominant ionization stage in coronal plasmas at temperatures above 20,000 K and is important at 15,000 K. Thus, we are not surprised to see a substantial amount of  $\text{Si}^{++}$  at the limb of the exoplanet’s outflow where protons from the solar wind and planetary escape are present to ionize  $\text{Si}^+$ , but the amount of  $\text{Si}^{++}$  could vary appreciably with changes in the stellar wind, planetary mass-loss rate, and temperature of the gas escaping from the planet’s exosphere.

### 3.4. *Is There Velocity Structure in the Planet’s Mass Loss?*

Until now we have discussed the mean transit/non-transit flux ratios for the entire line cores between  $-50$  and  $+50$   $\text{km s}^{-1}$ , but there are indications of departures from these mean ratios which indicate that the absorption in the planet’s mass loss depends on velocity. To test this idea, we compare in Figure 4 the difference and ratio profiles for the Si III and co-added C II lines. We find deep absorption features near  $-10$  and  $+15$   $\text{km s}^{-1}$  in both lines that are larger than the indicated errors shown in Figures 2 and 3. Since the C II and Si III lines are likely formed in the same region of the exosphere, we include in Figure 4 the co-addition of the two profiles with typical error bars for comparison with theoretical models. The increase in S/N with the co-addition of the C II and Si III spectra allows us to make more definitive statements about the velocity structure. The dips near  $-10$  and  $+15$   $\text{km s}^{-1}$  are more than twice as large as the errors per spectral resolution element (about 17  $\text{km s}^{-1}$ ) and are most likely real. In addition, the ratios near  $-40$  and  $+30$ – $70$   $\text{km s}^{-1}$  are also low, but the line fluxes decrease rapidly away from line center and these low ratios are less certain. Future observations with higher S/N are needed to confirm this first detection of velocity structure in the expanding atmosphere of an exoplanet. We also note that there are absorption features near  $+20$  and  $+40$   $\text{km s}^{-1}$  in the transit/non-transit ratio for the Si IV line which are greater than the noise level. Future observations are also needed to test the reality of these features.

### 3.5. Does HD 209458b have a Comet-like Tail?

Schneider et al. (1998) proposed that giant exoplanets located close to their host star will have comet-like tails of ionized gas produced by the interaction of the stellar wind and ions escaping from the planet’s exosphere, and that these tails could produce absorption when observed in front of the star. Vidal-Madjar et al. (2003) then predicted that stellar Lyman- $\alpha$  radiation pressure on hydrogen atoms escaping from the planet’s exosphere would form a comet-like tail trailing the planet. The presence of gas in an extended tail should produce more absorption at and beyond egress than during ingress phases. Schneiter et al. (2007) calculated possible cometary wakes and the time evolution of Lyman- $\alpha$  absorption from ingress to beyond egress. We searched our C II and Si III spectra for line profile differences between the ingress and egress phases to see whether these ions could be present in significant amounts in a tail, but we found no differences larger than the noise level. Future observations with higher S/N are required to verify the predictions of comet-like tails.

## 4. MASS-LOSS RATE IN A THERMAL PLASMA OUTFLOW

The  $\approx 8 \pm 1\%$  obscuration of the star in the C II and Si III lines during transit far exceeds the 1.5% obscuration by the exoplanet’s disk, indicating absorption by an extended atmosphere or mass loss that is optically thick in the C II and Si III lines. Our result for the C II lines is consistent with the  $7.5_{-3.4}^{+3.6}\%$  absorption depth that Vidal-Madjar et al. (2004) obtained for the unresolved C II lines, but very different from the absorption depth of  $0.0_{-0.0}^{+2.2}\%$  that they obtained for the Si III line. Their absorption depth of  $0.0_{-0.0}^{+6.5}\%$  for the Si IV line is consistent with our result.

Since the size of the obscuring material (optically thick in these lines) is similar to the size of the exoplanet’s Roche lobe (Ben-Jaffel & Sona Hosseini 2010), one possible explanation for the transit data is that the Roche lobe is filled by mass loss from the planet. Another possible explanation is that the exoplanet’s escaping gas forms an extended cometary tail blown out by the stellar wind, as suggested by hydrodynamical simulations (Schneiter et al. 2007).

We estimate the mass-loss rate from the planet’s atmosphere by assuming that the outflow forms a spherically symmetric envelope around the planet which is optically thick in the C II resonance line covering about 8% of the stellar surface. The spherical symmetry assumption is a good approximation because the shape of the tidally induced Roche lobe as seen during transit is close to a sphere (Lecavelier des Etangs et al. 2004). The envelope becomes optically thin at its “limb” because gas expansion and mass flux conservation reduce

the gas density with increasing radial distance ( $r$ ) from the planet. We define the envelope “limb” to be at the radial distance from the planet for which the absorption area is the same as that of an opaque sphere of the same size.

We consider a line of sight from the star that passes through the envelope with  $p$  the point of closest approach to the planet. The quantity  $x$  measures the distance along this line of sight from point  $p$  back to the star. The optical depth to the observer in the C II resonance line along this line of sight at the apparent limb of the envelope is,

$$\tau(p, \Delta\nu) = 2k \int_0^\infty n_{C II}(x) dx = 0.69, \quad (1)$$

where  $n_{C II}$  is the number density of C<sup>+</sup> ions,  $k = \frac{\sqrt{\pi}e^2}{mc} \frac{f}{\Delta\nu_D}$  is the line opacity,  $f = 0.128$  is the oscillator strength,  $m$  is the electron mass, and  $\Delta\nu_D$  is the Doppler width. The value of  $p$  depends somewhat on the displacement from line center,  $\Delta\nu$ , because for expanding gas, most of the absorption occurs near the frequency corresponding to the line-of-sight component of the expansion velocity. The limb occurs at  $\tau = 0.69$ , where as much stellar flux is transmitted through the envelope for lines of sight passing inside of  $p$  as for those lines of sight passing outside of  $p$ ,  $\int_{0.69}^\infty e^{-t} dt = \int_0^{0.69} e^{-t} dt$ , where  $t$  is the optical depth through the envelope for lines of sight with different values of  $p$ . Since the gas density and thus optical depth increase along lines of sight inside of  $p$ , the limb will occur at somewhat smaller optical depths depending on details the density and outflow velocity. For example, Lecavelier des Etangs et al. (2008a) calculated  $\tau = 0.56$  for an atmosphere in hydrostatic equilibrium, which has a density that decreases exponentially outward but does not have an outflow or heating in the outer layers. If the density decreases with radial position according to a power law, then  $\tau$  could be smaller than 0.69 by a factor of 2 or 3. The resulting mass loss rates would also be smaller by this factor. We call attention to this uncertainty that should be with resolved by realistic models based on physical principles that predict transit line profiles consistent with the COS data.

Since the gas density decreases with increasing radial distance from the planet  $r$  (thus increasing  $x$  along the line of sight),  $p$  should decrease slightly with increasing  $\Delta\nu$ . We compute  $\Delta\nu_D = 2.7 \times 10^{10} \text{ s}^{-1}$ , assuming a gas temperature of 10,000 K (Garcia Muñoz 2007; Ballester et al. 2007). If the outflow is turbulent or some absorbers have superthermal velocities (see below), then  $\Delta\nu_D$  will be larger. For a spherical outflow with constant mass flux, the mass flux of C<sup>+</sup> ions from the planet is

$$\dot{M}_{C II} = 4\pi r^2 m_C v n_{C II}(r), \quad (2)$$

where  $v$  is the outflow speed at  $r$ ,  $m_C$  is the mass of a carbon atom, and  $r^2 = x^2 + p^2$ .

We estimate  $\dot{M}_{C II}$  by requiring that the gas in the exosphere obscure 8% of the stellar disk within  $\Delta\nu_D$  of line center, corresponding to  $\pm 3.7$  km s<sup>-1</sup>. This condition will occur when the optical depth is about 0.69 at  $p^2 = 0.08R_\star^2$ , i.e.,

$$\tau(p = 0.284R_\star, \Delta\nu) = \frac{2\sqrt{\pi}e^2 f \dot{M}_{C II}}{mc\Delta\nu_D 4\pi m_C v} \int_0^\infty \frac{dx}{r^2} = 0.69. \quad (3)$$

The integral has an analytical solution by setting  $u = x/p$  of

$$\int_0^\infty \frac{dx}{r^2} = \frac{1}{p} \int_0^\infty \frac{du}{u^2 + 1} = \frac{\pi}{2p}. \quad (4)$$

We adopt  $v = 10$  km s<sup>-1</sup> at  $p = 0.284R_\star = 2.36R_{planet}$  from the theoretical models of Tian et al. (2005), Garcia Muñoz (2007), and Murray-Clay et al. (2009). We then find that

$$\dot{M}_{C II} = 2.1 \times 10^7 \text{ g s}^{-1} = 6.8 \times 10^{14} \text{ g yr}^{-1}. \quad (5)$$

In his model for the exosphere of HD 209458b, Garcia Muñoz (2007) found that essentially all of the carbon is singly ionized. If we assume that the carbon abundance is solar,  $2.7 \times 10^{-4}$  that of hydrogen (Asplund et al. 2009), the total mass-loss rate from the planet for only thermal broadening of the C II lines is

$$\dot{M}_{total} = 8.0 \times 10^{10} \text{ g s}^{-1} = 2.4 \times 10^{18} \text{ g yr}^{-1}. \quad (6)$$

Since the planet’s mass is  $1.2 \times 10^{30}$  g (Knutson et al. 2007), the fractional mass-loss rate per year is very small, as shown by

$$\frac{\dot{M}_{total}}{M_{planet}} = 2.0 \times 10^{-12} \text{ yr}^{-1}. \quad (7)$$

This calculation assumes that the mass-loss rate and planetary orbit do not change with time. Since additional line broadening is required to explain the broad absorption in the C II lines, these values of  $\dot{M}_{C II}$  and  $\dot{M}_{total}$  are at the lower end of their realistic ranges (see Section 5).

## 5. DISCUSSION

We now compare our empirical mass-loss rate with those of various theoretical models. All theoretical models of which we are aware assume hydrodynamical outflow driven by high temperatures and pressures near the base of the outflow. The important questions are the amount and location of energy absorbed from the star, the important cooling mechanisms, and the location of the sonic point in these transonic (Parker-like) winds relative to the location of the exoplanet’s Roche lobe. Vidal-Madjar et al. (2003) demonstrated that neutral hydrogen must be escaping from a volume larger than the planet’s Roche lobe by an unspecified mass-loss mechanism and that stellar radiation pressure further accelerates the outflow and shapes a comet-like tail. They proposed that the mass-loss rate is  $\dot{M} > 10^{10}$  g s<sup>-1</sup>, but they added that “owing to saturation effects in the [Lyman- $\alpha$ ] absorption line, a flux larger by several orders of magnitude would produce a similar absorption signature.” Murray-Clay et al. (2009) computed models with and without radiation pressure and concluded that radiation pressure does not increase  $\dot{M}$ , but it can change the location of the mass loss from the day side to the night side of the exoplanet. Tidal forces also do not change  $\dot{M}$  appreciably, but they move the sonic point closer to the exoplanet and increase the flow velocity (Garcia Muñoz 2007; Murray-Clay et al. 2009).

All of the theoretical models assume that HD 209458 is a main sequence star like the Sun with ultraviolet and extreme ultraviolet radiative output similar to the Sun at low or high activity. Since mass-loss rates are proportional to the energy input (the so-called energy-limited escape rate), the critical question is the energy input rate. In all of the models, expansion (PdV work) is the dominant cooling mechanism, although radiation by H<sub>3</sub><sup>+</sup> at the base of the flow must be included (Yelle 2004), and radiation in the Lyman- $\alpha$  line can be important for T Tauri star radiative input rates. Many models assume that only the energy remaining after stellar Lyman continuum (E > 13.6 eV) photons ionize neutral hydrogen is available to energize the outflow, so that the assumed fraction of this radiation (83% or 100% in different models) controls the outflow. For such models,  $\dot{M}$  is a few times 10<sup>10</sup> g s<sup>-1</sup>. For example, Yelle (2004), as corrected in Yelle (2006), finds  $\dot{M} = 4.7 \times 10^{10}$ , Tian et al. (2005) find  $\dot{M} < 6 \times 10^{10}$ , Garcia Muñoz (2007) finds  $\dot{M} = 6.1 \times 10^{10}$  for EUV flux similar to the low activity Sun but  $\dot{M} = 1.5 \times 10^{11}$  for EUV flux like the active Sun. Murray-Clay et al. (2009) find that  $\dot{M} \sim 2 \times 10^{10}$  g s<sup>-1</sup>.

The inclusion of atoms and molecules other than H, H<sup>+</sup>, and H<sub>2</sub> can significantly change the outflow, in particular by increasing the mass-loss rate, because more of the stellar UV radiation is available to heat the outflow and drive the mass loss. For example, the Lyman- $\alpha$  line contains more flux than the entire Lyman continuum (Ribas et al. 2005), and other UV emission lines and continuum radiation in the wavelength range 912–2000 Å can be

absorbed in the bound-free continua of atomic species (e.g., CNO) and molecules including  $\text{H}_2$ . When Garcia Muñoz (2007) added solar abundances of CNO to his models,  $\dot{M}$  increased by a factor of 4.5 (see his Table 6). Including partial absorption of the 1000–2000 Å stellar flux by atoms and molecules with solar abundances increases  $\dot{M}$  to  $6.3 \times 10^{11} \text{ g s}^{-1}$ . Metals must exist in the distant outflow since we see absorption during transit in the C II and Si III lines. By equating the energy input of both Lyman continuum and Lyman- $\alpha$  with stellar fluxes estimated from the rotation rate of HD 209458, Lecavelier des Etangs (2007) found  $\dot{M} \sim 3 \times 10^{11} \text{ g s}^{-1}$ . Using a similar energy balance argument, Lammer et al. (2003) obtained  $\dot{M} \sim 3 \times 10^{11} \text{ g s}^{-1}$ , but Yelle (2004) suggested that this result could be an overestimate as a result of not including  $\text{H}_3^+$  cooling and ionization of H.

A critical question is whether line absorption during transit is produced entirely by the outflowing thermal plasma or whether high-velocity atoms and ions (either at higher temperatures or nonthermal) are required to explain the broadest part of the absorption line profiles. Ben-Jaffel & Sona Hosseini (2010) show that neutral hydrogen absorption by scaled hydrodynamic outflow models may explain the flux decrease during transit even at  $\pm 100 \text{ km s}^{-1}$  from the center of the Lyman- $\alpha$  line, but such models predict much less absorption during transit than is detected in the unresolved O I and C II line flux measurements (Vidal-Madjar et al. 2004). Additional high-velocity absorbers are needed to explain the O I, C II, and probably also the Lyman- $\alpha$  data, but there is no agreement concerning the source of the high-velocity absorbers. One possibility is radiation pressure, but Murray-Clay et al. (2009) argue that the observed absorption near  $+100 \text{ km s}^{-1}$  from the center of the Lyman- $\alpha$  line is difficult to explain by stellar radiation pressure as originally proposed by Vidal-Madjar et al. (2003). However, radiation pressure on neutral hydrogen atoms must be present, and Lecavelier des Etangs et al. (2008b) argue that radiation pressure by itself can explain the Lyman- $\alpha$  observations. Holmström et al. (2008) and Murray-Clay et al. (2009) argue that the observed decrease in Lyman- $\alpha$  flux near and beyond  $\pm 100 \text{ km s}^{-1}$  during transit requires high-velocity H atoms that could be explained by charge exchange between stellar wind protons and neutral H atoms in the exoplanet’s outflow. These high-velocity H atoms are called ENAs (energetic neutral atoms).

Ben-Jaffel & Sona Hosseini (2010) have tested whether the presence of high-velocity atoms and ions could explain the flux reduction observed in the unresolved O I and C II line transit data. They assume that a portion of the gas has an effective temperature (either thermal or nonthermal) many times larger than the thermal temperature in outflow models. For the unresolved C II 1334, 1335 Å multiplet, they can explain the observed flux reduction by  $\text{C}^+$  ions with effective temperatures 5.5–107 times larger than the background gas temperature ( $T_B$ ) in typical hydrodynamic models depending on the properties of the outflow models and the assumed location of the  $\text{C}^+$  ions. In Figure 9 of their paper, they

show examples of predicted C II 1334 Å line profiles during transit with  $T_{CII}/T_B \sim 16$  and  $\sim 28$  that can explain the total decrease in unresolved line flux during transit, but these particular examples are either too narrow or triangular in shape, unlike the observed C II line profiles which show significant flux reduction between  $-50$  and  $+50$  km s $^{-1}$  with probable enhanced absorption near  $-10$  and  $+15$  km s $^{-1}$ . Ben-Jaffel (private communication) informs us that other models with somewhat larger  $T_{CII}/T_B$  ratios can explain the flat reduction in C II line flux between  $-50$  and  $+50$  km s $^{-1}$ . However these models have *ad hoc* velocity distributions and they do not explain the observed velocity structure. In their paper, they conclude that COS spectra are needed to “...reveal the true balance between thermal and non-thermal populations...”. We encourage the development of new models, preferably based on plausible physical mechanisms, to explain the observed line profiles.

Our analysis of the C II line absorption during transit assuming only thermal absorption by 10,000 K gas and solar carbon abundance led to our estimate of  $\dot{M}_{total} = 8.0 \times 10^{10}$  g s $^{-1}$ . This mass-loss rate is somewhat larger than the theoretical estimates mentioned above that assume an outflow with no metals. The assumption of no metals in the outflow is clearly unrealistic as we observe absorption by C II and Si III at  $2.36R_{planet}$ . At the same time, our analysis of the C II lines assuming only thermal line broadening (at 10,000 K) is unrealistic as the thermal velocity is only 3.7 km s $^{-1}$ , and we observe absorption out to  $\pm 50$  km s $^{-1}$ . Since we measure the mass flux at the limb of the outflow where the C II optical depth is small ( $\tau = 0.69$ ), we cannot invoke optical thickness to explain the broad profile. Note that the same is true for the Lyman- $\alpha$  line, but (as the referee has called to our attention) Ben-Jaffel & Sona Hosseini (2010) and other authors include opacity and Lorentzian line shapes at the limb as a possible mechanism for absorption line broadening.

Equation 3 shows that  $\dot{M}_{CII}$  is proportional to the Doppler broadening parameter  $\Delta\nu_D$ . To obtain 8% absorption at  $\pm 50$  km s $^{-1}$  from line center requires either turbulent broadening with velocity of about 50 km s $^{-1}$  or superthermal C $^+$  ions with similar velocities. If turbulent broadening is responsible, then the mass-loss rate increases by a factor of 13 to  $\dot{M}_{total} = 1 \times 10^{12}$  g s $^{-1}$ . However, 50 km s $^{-1}$  turbulent velocities are highly supersonic and unlikely. We estimate that a sensible upper limit to the turbulent velocity would be twice the flow speed or 20 km s $^{-1}$ , for which  $\dot{M}_{total} \approx 4 \times 10^{11}$  g s $^{-1}$ . This would increase  $\dot{M}_{total}/M_{planet}$  to  $\approx 4 \times 10^{-11}$  yr $^{-1}$ .

If high-velocity C $^+$  ions are responsible for the broad absorption, then the mass-loss rate could be closer to the thermal value because only a small fraction of the C $^+$  ions are likely to have high velocities. We conclude that  $\dot{M}_{total} = (8-40) \times 10^{10}$  g s $^{-1}$  is consistent with the C II line profiles. We find it interesting that when Garcia Muñoz (2007) includes metals with solar abundances in his hydrodynamic mass outflow models, the mass-loss rate

increases from  $\dot{M} = 1.4 \times 10^{11}$  to  $\dot{M} = 4.95 \times 10^{11}$  g s<sup>-1</sup>, a value near the top end of our empirical mass-loss rate estimate. Thus high-velocity C<sup>+</sup> ions are required to explain the C II absorption during transit. Similar arguments would likely explain the broad Si III transit absorption.

## 6. CONCLUSIONS

The high sensitivity and moderate spectral resolution of COS allowed us to obtain the first measurements of gas absorption in the exosphere of a transiting exoplanet in lines of C II and Si III with velocity resolution. During transits of HD 209458, we found that the mean flux in these lines is reduced by  $7.8 \pm 1.3\%$  for the co-added C II lines and  $8.2 \pm 1.4\%$  for the Si III line in the velocity range  $-50$  to  $+50$  km s<sup>-1</sup>. The 8% absorption constraint sets the location of the outflow limb ( $2.36R_{planet}$ ) where the C II lines become optically thin. Theoretical hydrodynamic models show that the outflow velocity is about 10 km s<sup>-1</sup> and gas temperature about 10,000 K at this location. If we assume that the outflow is purely thermal, then  $\dot{M}_{total} = 8 \times 10^{10}$  g s<sup>-1</sup>, somewhat larger than theoretical estimates based on outflows with no metals. Since absorption in the C II lines is much broader than indicated by Doppler broadening with a thermal velocity of 3.7 km s<sup>-1</sup>, the lines must be broadened by large turbulence or high-velocity C<sup>+</sup> ions. If turbulent broadening dominates, then the 8% absorption seen out to  $\pm 50$  km s<sup>-1</sup> would require mass-loss rates as large as  $1 \times 10^{12}$  g s<sup>-1</sup>, but such highly supersonic velocities are not likely. Instead, absorption by high-velocity C<sup>+</sup> and Si<sup>++</sup> ions formed by the interaction of the stellar wind and planetary mass loss or some other mechanism broadens the C II and Si III lines. We conclude that the mass-loss rate in the exoplanet’s outflow is in the range  $(8-40) \times 10^{10}$  g s<sup>-1</sup>. These rates assume that the carbon abundance is solar, which is not the case for the giant planets in the solar system. We note that mass-loss rates predicted by hydrodynamic models that include solar abundant metals in the outflow lie at the upper limit of this range.

Comparison of the C II and Si III line depths and transit/non-transit line ratios shows deep absorption features near  $-10$  and  $+15$  km s<sup>-1</sup> in both lines. Since the C II and Si III lines are likely formed in the same region of the exosphere, we include in Figure 4 the co-addition of the two profiles with typical error bars for comparison with theoretical models. The increase in S/N with the co-addition of the C II and Si III spectra allows us to make more definitive statements about the velocity structure. The dips near  $-10$  and  $+15$  km s<sup>-1</sup> are more than twice as large as the errors per spectral resolution element (about 17 km s<sup>-1</sup>) and are most likely real. In addition, the ratios near  $-40$  and  $+30-70$  km s<sup>-1</sup> are also low, but the line fluxes decrease rapidly away from line center and these low ratios are less certain.



Future observations with higher S/N are needed to confirm this first detection of velocity structure in the expanding atmosphere of an exoplanet.

The COS transit observations of the absorption velocity structure in these lines demonstrate the need for including high-velocity  $C^+$  and  $Si^{++}$  ions in models of the exosphere of HD 209458b and presumably other close-in exoplanets. It remains to be seen whether the inclusion of a simple distribution of ions with high effective temperature as proposed by Ben-Jaffel & Sona Hosseini (2010) is adequate to explain the data. The new COS data provide the opportunity to test a range of absorption models based on such physical mechanisms as radiation pressure, charge exchange, and interactions between the stellar wind and the planet’s outflow to understand mass-loss processes in the exospheres of close-in planets.

This work is supported by NASA through grants NNX08AC146 and NAS5-98043 to the University of Colorado at Boulder. We thank the many people at the Space Telescope Science Institute, Goddard Space Flight Center, Ball Aerospace and Technologies Corp. and CASA at the University of Colorado for the excellent hardware and software that has made COS a great success. We particularly wish to thank the referee for his many thoughtful and thorough comments and his bringing to our attention important publications that have led to significant modifications in the paper. We thank Dr. J. Schneider for encouraging us to look for an asymmetry between ingress and egress. We also thank Dr. Lofti Ben-Jaffel for clarifying our understanding of the Ben-Jaffel & Hosseini (2010) paper. We thank Dr. Alain Lecavelier for calling our attention to the different values of  $\tau$  at the limb that depend on the density structure in the envelope.

## REFERENCES

- Asplund, M., Grevesse, N., Sauval, J., & Scott, P. 2009, *ARA&A*, 47, 481
- Baliunas, S. L. & Butler, S. E. 1980, *ApJ*, 235, L45
- Ballester, G. E., Sing, D. K., & Herbert, F. 2007, *Nature*, 445, 511
- Baraffe, I., Selsis, F., Chabrier, G., Barman, T. S., Allard, F., Hauschildt, P. H., & Lammer, H. 2004, *A&A*, 419, L13
- Ben-Jaffel, L. 2007, *ApJ*, 671, L61
- Ben-Jaffel, L. 2008, *ApJ*, 688, 1352
- Ben-Jaffel, L. & Sona Hosseini, S. 2010, *ApJ*, 709, 1284

- Charbonneau, D., Brown, T. M., Latham, D., & Mayor, M. 2000, *ApJ*, 529, L45
- Charbonneau, D., Brown, T. M., Noyes, R. W., & Gilliland, R. L. 2002, *ApJ*, 568, 377
- Ehrenreich, D. et al. 2008, *A&A*, 483, 933
- Garcia Muñoz, A. 2007, *Planet. Space Sci.*, 55, 1426
- France, K., Stocke, J. T., Yang, H., Linsky, J. L., Froning, C. S., Green, J. C., & Osterman, S. N. 2010, *ApJ*, to appear
- Ghavamian, P. et al. 2010 *BAAS*, 42, 499
- Henry, G. W., Marcy, G. W., Butler, R. P., & Vogt, S. S. 2000, *ApJ*, 529, L41
- Holmström, M., Ekenbäck, A., Selsis, F., Penz, T., Lammer, H., & Wurz, P. 2008, *Nature*, 451, 970
- Jaritz, G. F., Endler, S., Langmayr, D., Lammer, H., Griessmeier, J.-M., Erkaev, N. V., & Biernat, H. K. 2005, *A&A*, 439, 771
- Koskinen, T. T., Aylward, A. D., & Miller, S. 2007, *Nature*, 450, 845
- Koskinen, T. T., Yelle, R. V., Lavvas, P., & Lewis, N. K. 2010, arXiv:1004.1396
- Knutson, H. A., Charbonneau, D., Noyes, R. W., Brown, T.M., & Gilliland, R. L. 2007, *ApJ*, 655, 564
- Lammer, H., Selsis, F., Ribas, I., Guinan, E. F., Bauer, S. J., & Weiss, W. W. 2003, *ApJ*, 598, L121
- Lecavelier des Etangs, A. 2007, *A&A*, 461, 1185
- Lecavelier des Etangs, A., Vidal-Madjar, A., McConnell, J. C., & Hébrard, G. 2004, *A&A*, 418, L1
- Lecavelier des Etangs, A., Pont, F., Vidal-Madjar, A., & Sing, D. 2008a, *A&A*, 481, L83
- Lecavelier des Etangs, A., Vidal-Madjar, A., & Desert, J.-M. 2008b, *Nature*, 458, E1
- Mazeh, T. et al. 2000, *ApJ*, 532, L55
- Murray-Clay, R. A., Chiang, E. I., & Murray, N. 2009, *ApJ*, 693, 23
- Redfield, S. & Linsky, J. L. 2008, *ApJ*, 673, 283

- Ribas, I., Guinan, E. F., Güdel, M., & Audard, M. 2005, *ApJ*, 622, 680
- Rottman, G. 2006, *Space Sci. Rev.*, 125, 39
- Schneider, J., Rauer, H., Lasota, J. P., Bonazzola, S., & Chassefière, E. 1998, in *ASP Conf. Series 134, Brown Dwarfs and Extrasolar Planets*, ed. R. Rebolo, E. L. Martín, & M. R. Zapatero Osorio (San Francisco, ASP), 241
- Schneider, E. M., Velázquez, P. F., Esquivel, A., Raga, A. C., & Blanco-Cano, X. 2007 *ApJ*, 671, 57
- Tian, F., Toon, O. B., Pavlov, A. A., & De Sterck, H. 2005, *ApJ*, 621, 1049
- Wittenmyer, R. A. et al. 2005, *ApJ*, 632, 1157
- Vidal-Madjar, A. et al. 2003, *Nature*, 422, 143
- Vidal-Madjar, A. et al. 2004, *ApJ*, 604, L69
- Vidal-Madjar, A., Lecavelier des Etangs, A., Désert, J.-M., Ballester, G. E., Ferlet, R., Hébrard, G., & Mayor, M. 2008, *ApJ*, 676, L57
- Yelle, R. V. 2004, *Icarus*, 170, 167
- Yelle, R. V. 2006, *Icarus*, 183, 508

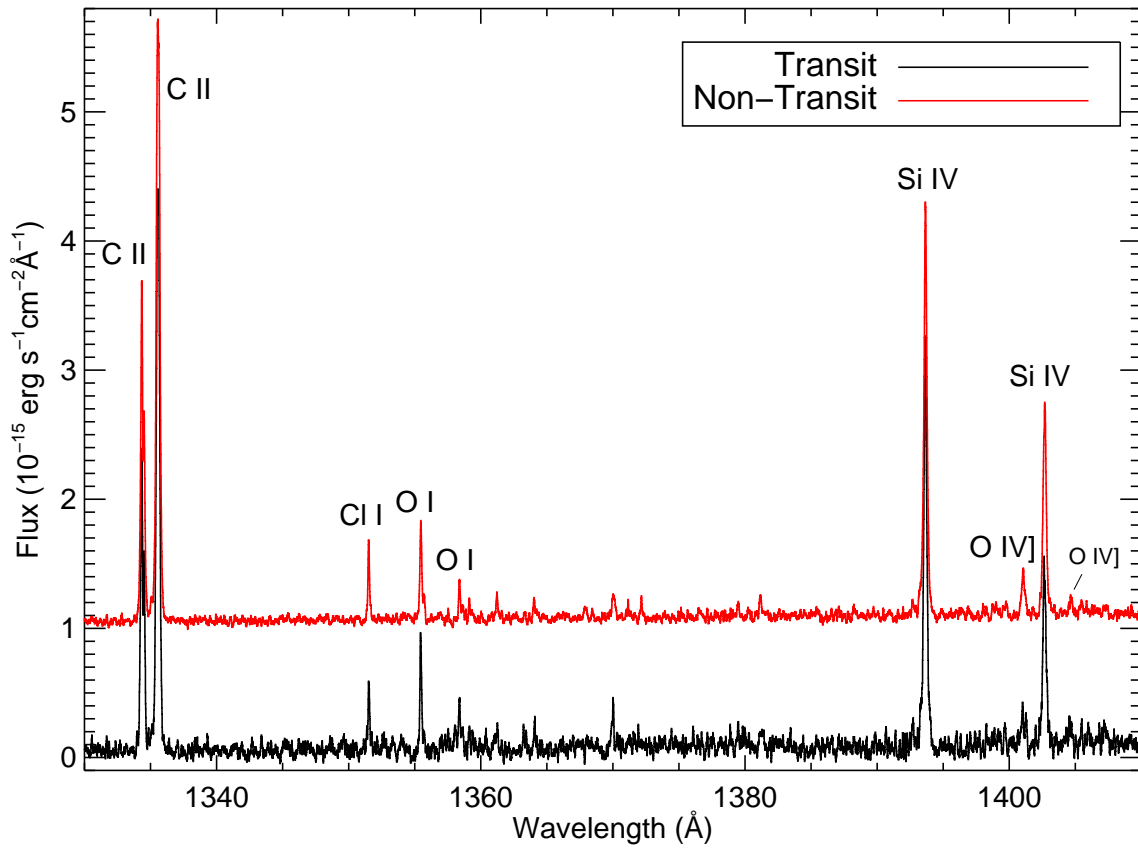


Fig. 1.— A portion of the COS G130M spectrum of HD 209458. The lower (black) plot is the sum of four spectra obtained during transit. The upper (red) plot (displaced upward) is the sum of the ten quadrature and four secondary eclipse spectra.

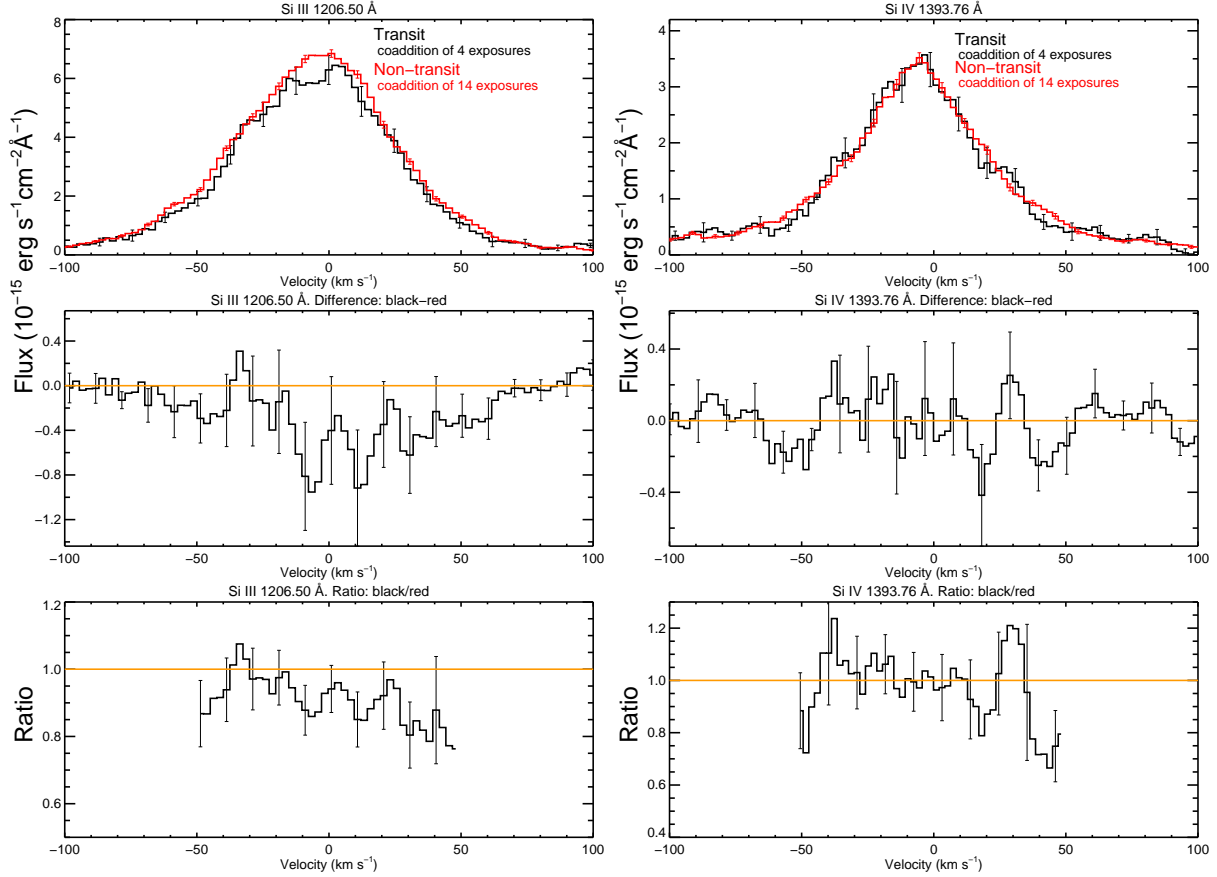


Fig. 2.— Upper panels: Comparison of the four co-added spectra obtained during transit (black) with the co-added non-transit spectra (red) for the Si III and Si IV lines. Representative error bars per pixel are included. Middle panels: difference spectra (transit minus non-transit) with representative error bars. Lower panels: flux ratio (transit/non-transit) spectra. The ratios are not plotted beyond  $\pm 50$  km s $^{-1}$  as the errors are large at low flux levels. The velocity scale is relative to the  $-14.8$  km s $^{-1}$  radial velocity of the star.

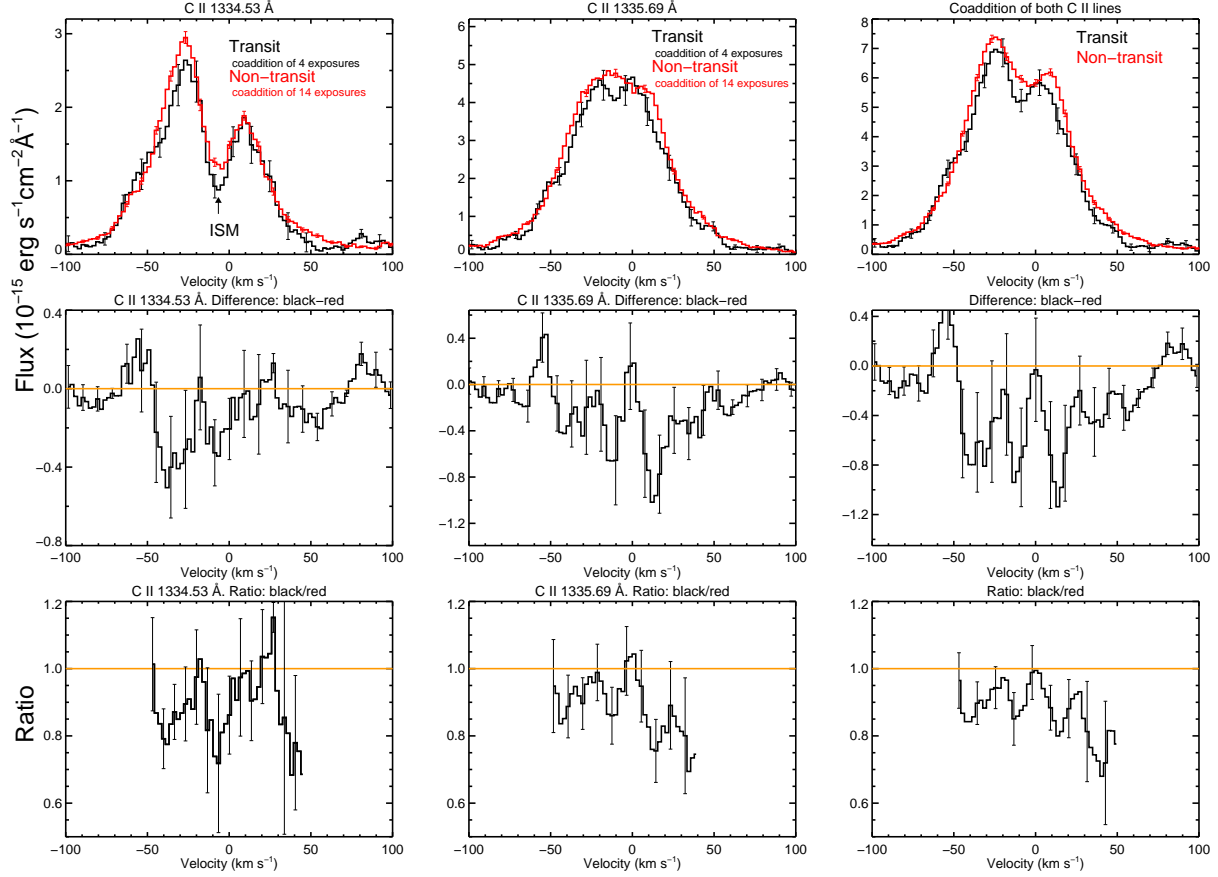


Fig. 3.— Upper panels: Comparison of the four co-added spectra obtained during transit (black) with the co-added non-transit spectra (red) for the C II 1334.53 Å and 1335.69 Å lines. The upper right panel show a co-addition of both C II lines on the same velocity scale. Representative error bars per pixel are included. Middle panels: difference spectra (transit minus non-transit) with representative error bars for each C II line and the combined C II line. Lower panels: flux ratio (transit/non-transit) spectra. The ratios are not plotted beyond  $\pm 50$  km s $^{-1}$  as the errors are large at low flux levels. The velocity scale is relative to the  $-14.8$  km s $^{-1}$  radial velocity of the star.

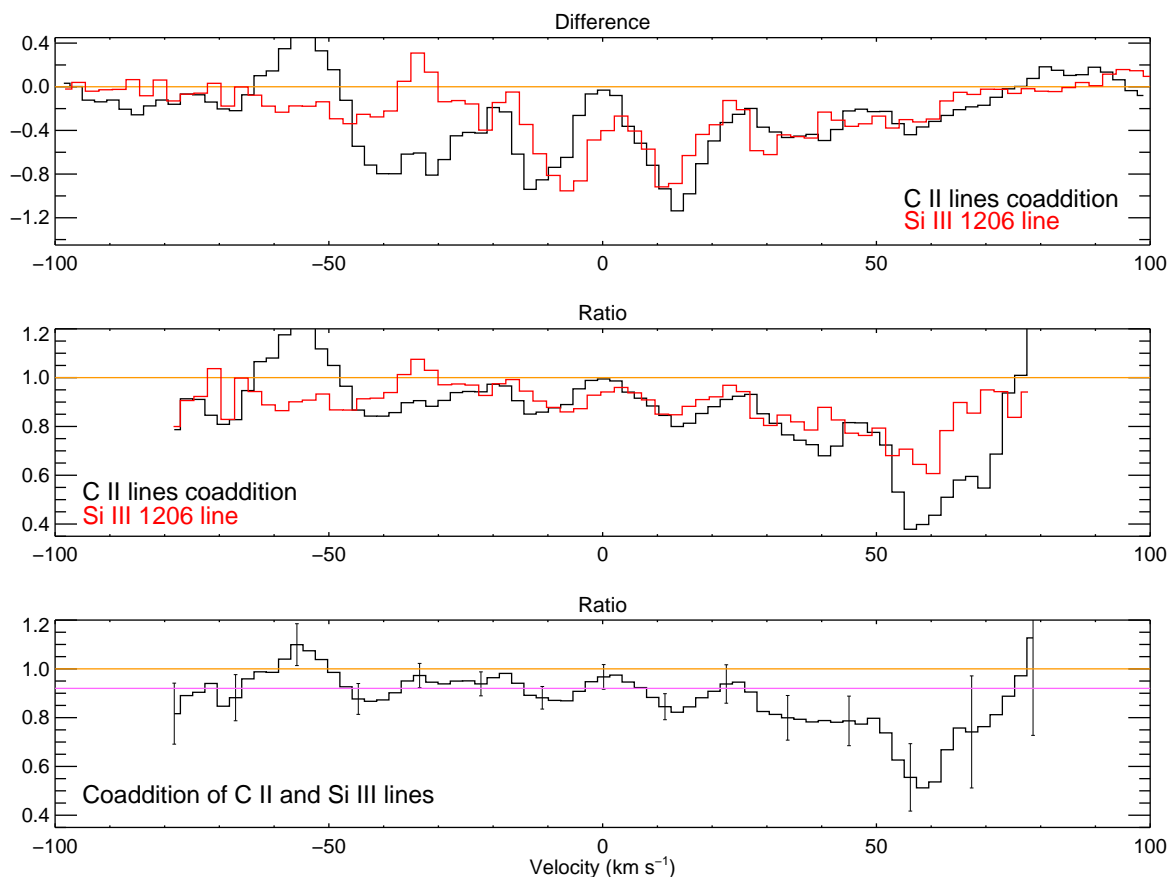


Fig. 4.— Upper and middle panels: Comparison of the difference spectra (transit minus non-transit) and ratio spectra (transit/non-transit) for the co-addition of the C II Lines (black) and the Si III line (red). Lower panel: Co-addition of the C II and Si III ratio spectra with typical errors per spectral resolution element (about 17 km s<sup>-1</sup>). The horizontal line at 0.92 is the mean ratio for the velocity interval -50 to +50 km s<sup>-1</sup>. The dips near -10 and +15 km s<sup>-1</sup> are each more than 2 $\sigma$  and likely real. The low ratio features near -40 and +30–70 km s<sup>-1</sup> occur where the line fluxes are low and are thus less certain.

Table 1. Properties<sup>a</sup> of HD 209458 and HD 209458b

Spectral type	G0 V
Distance (pc)	47
$M_{\star}/M_{\odot}$	$1.101^{+0.066}_{-0.062}$
$R_{\star}/R_{\odot}$	$1.125^{+0.020}_{-0.023}$
$P_{\text{orbit}}$ (days)	3.52474859(38)
$R_{\text{planet}}/R_{\text{Jup}}$	$1.320^{+0.024}_{-0.025}$
$M_{\text{planet}}/M_{\text{Jup}}$	$0.64 \pm 0.06$
$\rho_{\text{planet}}/\rho_{\text{Jup}}$	$0.26 \pm 0.04$
Semimajor axis (AU)	0.045
Stellar flux at planet/Jupiter	13,400
Escape speed (km/s)	$42 \pm 4$
Orbital Velocity ampl. (km/s)	146
Transit duration (hr)	3.22
Transit depth for $R_{\text{planet}}$	1.5%
Transit depth for $R_{\text{Roche}}$	10%

<sup>a</sup>Data from Knutson et al. (2007).



Table 2. COS G130M Observations of HD 209458 (Program 11534)

Exp. Time (s)	Phase	Day	Start	Stop	Gap <sup>a</sup> (Å)
2340.2	0.2516–0.2593	19 Sep	10:10:15	10:49:15	1278–1290
0955.2	0.2684–0.2716	19 Sep	11:35:37	11:51:32	1288–1299
1851.2	0.2722–0.2782	19 Sep	11:54:40	12:25:31	1296–1306
0560.0	0.2873–0.2891	19 Sep	13:11:29	13:20:49	1288–1299
2235.1	0.2898–0.2971	19 Sep	13:24:06	14:01:21	1306–1316
2340.2	0.7059–0.7136	24 Sep	13:12:09	13:51:09	1278–1290
0945.2	0.7229–0.7260	24 Sep	14:38:04	14:53:49	1288–1299
1787.2	0.7266–0.7324	24 Sep	14:56:57	15:26:44	1296–1306
0925.2	0.7417–0.7448	24 Sep	16:13:54	16:29:19	1288–1299
1798.2	0.7454–0.7513	24 Sep	16:32:36	17:02:34	1306–1316
1045.2	0.9913–0.9947	02 Oct	14:32:10	14:49:35	1278–1290
1096.2	0.9954–0.9990	02 Oct	14:52:52	15:11:08	1288–1299
1400.2	0.0077–0.0123	02 Oct	15:55:28	16:18:48	1296–1306
1405.2	0.0129–0.0175	02 Oct	16:21:56	16:45:21	1306–1316
1057.2	0.4880–0.4915	18 Oct	10:57:04	11:14:41	1278–1290
1093.1	0.4921–0.4957	18 Oct	11:17:49	11:36:02	1288–1299
1401.2	0.5043–0.5089	18 Oct	12:19:37	12:42:58	1296–1306
1405.2	0.5095–0.5141	18 Oct	12:46:06	13:09:31	1306–1316

<sup>a</sup>The gap is the wavelength interval between the two detector faceplate elements. No data are available for the gap region, and there are instrumental artifacts at wavelengths close to the gap.